AFRL-AFOSR-VA-TR-2019-0076

Robust Data-Driven Aeroelastic Flight Envelope Tailoring

Balakumar Balachandran
MARYLAND UNIV COLLEGE PARK

03/27/2019
Final Report

Air Force Research Laboratory
AF Office Of Scientific Research (AFOSR)/ RTA2
Arlington, Virginia 22203
Air Force Materiel Command

REPORT DOCUMENTATION PAGE

Form Approved
OMB No. 0704-0188

PLEASE DO NOT RETURN YOUR FORM TO THE ABOVE ORGANIZATION.

1. REPORT DATE *(DD-MM-YYYY)*	**2. REPORT TYPE**	**3. DATES COVERED** *(From - To)*
03-22-2019	FINAL REPORT	06/01/2015-12/31/2018

4. TITLE AND SUBTITLE
Robust Data-Driven Aeroelastic Flight Envelope Tailoring

5a. CONTRACT NUMBER

5b. GRANT NUMBER
FA9550-15-1-0134

5c. PROGRAM ELEMENT NUMBER

6. AUTHOR(S)
B. Balachandran and S. Azarm

5d. PROJECT NUMBER

5e. TASK NUMBER

5f. WORK UNIT NUMBER

7. PERFORMING ORGANIZATION NAME(S) AND ADDRESS(ES)
Department of Mechanical Engineering
University of Maryland
College Park, MD 20742-3035

8. PERFORMING ORGANIZATION REPORT NUMBER

9. SPONSORING/MONITORING AGENCY NAME(S) AND ADDRESS(ES)
Dr. Erik Blasch
Program Manager, DDDAS
AFOSR/RTA-2
ARLINGTON, VA

10. SPONSOR/MONITOR'S ACRONYM(S)

11. SPONSOR/MONITOR'S REPORT NUMBER(S)

12. DISTRIBUTION/AVAILABILITY STATEMENT
DISTRIBUTION A: Distribution approved for public release.

13. SUPPLEMENTARY NOTES

14. ABSTRACT

The overall research objective was to develop and explore a dynamically data-driven decision support system to realize multi-objectively optimized system (joined-wing SensorCraft) stability under uncertainty. This project has resulted in a Dynamic Data Driven Application System (DDDAS) framework for a decision support system. This framework is composed of aeroelastic simulations, dynamic data-driven prediction, and operationally flexible robust optimization. Simulations are used to predict aeroelastic instabilities, which in turn are utilized in the prediction framework component to forecast the flutter boundaries for untested scenarios. An optimal design can then be constructed which best fits the predicted behaviors. Simulations are bolstered by the integration of the Fast Multipole Method (FMM) for computational reduction. Given that the aerodynamic calculations account for the majority of the computational cost, the aerodynamic calculations are accelerated through the FMM. A data-driven prediction framework was designed to include global, unsteady aeroelastic responses. In this framework, simulation data are integrated with measurement data from sparsely located sensors to make efficient and accurate predictions of unsteady responses of the system.

15. SUBJECT TERMS
DDDAS, aeroelasticity, active robust optimization, co-simulation, decision support system, sensor measurements, data assimilation, spatiotemporal response prediction, reduced-order modeling, Gaussian process, fast multipole method

16. SECURITY CLASSIFICATION OF:			**17. LIMITATION OF ABSTRACT**	**18. NUMBER OF PAGES**	**19a. NAME OF RESPONSIBLE PERSON**
a. REPORT	**b. ABSTRACT**	**c. THIS PAGE**			B. Balachandran
					19b. TELEPHONE NUMBER *(Include area code)* (301)405-5309

Reset

INSTRUCTIONS FOR COMPLETING SF 298

1. REPORT DATE. Full publication date, including day, month, if available. Must cite at least the year and be Year 2000 compliant, e.g. 30-06-1998; xx-06-1998; xx-xx-1998.

2. REPORT TYPE. State the type of report, such as final, technical, interim, memorandum, master's thesis, progress, quarterly, research, special, group study, etc.

3. DATES COVERED. Indicate the time during which the work was performed and the report was written, e.g., Jun 1997 - Jun 1998; 1-10 Jun 1996; May - Nov 1998; Nov 1998.

4. TITLE. Enter title and subtitle with volume number and part number, if applicable. On classified documents, enter the title classification in parentheses.

5a. CONTRACT NUMBER. Enter all contract numbers as they appear in the report, e.g. F33615-86-C-5169.

5b. GRANT NUMBER. Enter all grant numbers as they appear in the report, e.g. AFOSR-82-1234.

5c. PROGRAM ELEMENT NUMBER. Enter all program element numbers as they appear in the report, e.g. 61101A.

5d. PROJECT NUMBER. Enter all project numbers as they appear in the report, e.g. 1F665702D1257; ILIR.

5e. TASK NUMBER. Enter all task numbers as they appear in the report, e.g. 05; RF0330201; T4112.

5f. WORK UNIT NUMBER. Enter all work unit numbers as they appear in the report, e.g. 001; AFAPL30480105.

6. AUTHOR(S). Enter name(s) of person(s) responsible for writing the report, performing the research, or credited with the content of the report. The form of entry is the last name, first name, middle initial, and additional qualifiers separated by commas, e.g. Smith, Richard, J, Jr.

7. PERFORMING ORGANIZATION NAME(S) AND ADDRESS(ES). Self-explanatory.

8. PERFORMING ORGANIZATION REPORT NUMBER. Enter all unique alphanumeric report numbers assigned by the performing organization, e.g. BRL-1234; AFWL-TR-85-4017-Vol-21-PT-2.

9. SPONSORING/MONITORING AGENCY NAME(S) AND ADDRESS(ES). Enter the name and address of the organization(s) financially responsible for and monitoring the work.

10. SPONSOR/MONITOR'S ACRONYM(S). Enter, if available, e.g. BRL, ARDEC, NADC.

11. SPONSOR/MONITOR'S REPORT NUMBER(S). Enter report number as assigned by the sponsoring/ monitoring agency, if available, e.g. BRL-TR-829; -215.

12. DISTRIBUTION/AVAILABILITY STATEMENT. Use agency-mandated availability statements to indicate the public availability or distribution limitations of the report. If additional limitations/ restrictions or special markings are indicated, follow agency authorization procedures, e.g. RD/FRD, PROPIN, ITAR, etc. Include copyright information.

13. SUPPLEMENTARY NOTES. Enter information not included elsewhere such as: prepared in cooperation with; translation of; report supersedes; old edition number, etc.

14. ABSTRACT. A brief (approximately 200 words) factual summary of the most significant information.

15. SUBJECT TERMS. Key words or phrases identifying major concepts in the report.

16. SECURITY CLASSIFICATION. Enter security classification in accordance with security classification regulations, e.g. U, C, S, etc. If this form contains classified information, stamp classification level on the top and bottom of this page.

17. LIMITATION OF ABSTRACT. This block must be completed to assign a distribution limitation to the abstract. Enter UU (Unclassified Unlimited) or SAR (Same as Report). An entry in this block is necessary if the abstract is to be limited.

FINAL REPORT
AFOSR Grant FA9550-15-1-0134

Robust Data-Driven Aeroelastic Flight Envelope Tailoring

B. Balachandran (PI) and S. Azarm (Co-PI)
Research Participants: R. Kania, A. Kebbie-Anthony, and X. Zhao
Department of Mechanical Engineering
University of Maryland
College Park, MD 20742-3035

Abstract

The overall research objective was to develop and explore a dynamically data-driven decision support system to realize multi-objectively optimized system (joined-wing SensorCraft) stability under uncertainty. This project has resulted in a Dynamic Data Driven Application System (DDDAS) framework for a decision support system. This framework is composed of aeroelastic simulations, dynamic data-driven prediction, and operationally flexible robust optimization. Simulations are used to predict aeroelastic instabilities, which in turn are utilized in the prediction framework component to forecast the flutter boundaries for untested scenarios. An optimal design can then be constructed which best fits the predicted behaviors. Simulations are bolstered by the integration of the Fast Multipole Method (FMM) for computational reduction. Given that the aerodynamic calculations account for the majority of the computational cost, the aerodynamic calculations are accelerated through the FMM. The results obtained show a decrease of computational complexity from approximately $O\left(K^3\right)$ to $O\left(K^2\right)$ where K is the total number of time steps per simulation. A data-driven prediction framework was designed to include global, unsteady aeroelastic responses. In this framework, simulation data are integrated with measurement data from sparsely located sensors to make efficient and accurate predictions of unsteady responses of the system. Finally, an operationally flexible robust optimization methodology has been developed to utilize surrogate modeling for efficient use of available resources. Results obtained show that the surrogate modeling can help reduce the computations by several orders of magnitude.

Key words: DDDAS, aeroelasticity, active robust optimization, co-simulation, decision support system, sensor measurements, data assimilation, spatiotemporal response prediction, reduced-order modeling, Gaussian process, fast multipole method

Nomenclature

a	projected parameter element
$\mathbf{d}$	system's spatial location
$f(\bullet)$	system dynamic function
$g(\bullet)$	Gaussian process model
$\mathbf{g}$	constraint equation vector
I	number of simulated datasets
j	spatial location index
J	number of spatial locations
k	time step index
k_0	initial time step
K	total number of time steps
n	projected parameter index
N	number of vortex segments (sources)
$N(\bullet,\bullet)$	normal distribution function
N_b	size of relatively small body meshes
$\mathbf{p}_0$	nominal scenario parameters
$\mathbf{p}^*$	worst case scenario parameters
$\mathbf{P}$	set of all known scenarios
r_1	rank for spatial dimension
r_2	rank for temporal dimension
s_k	sensor measurement data at k^{th} time step
t	time step index within prediction framework
t_0	initial time step within prediction framework
V	freestream velocity of fluid
$\mathbf{V}$	eigen spatial matrices
$\mathbf{W}$	eigen temporal matrices
$\mathbf{x}$	system input
$\mathbf{x}_d^*$	optimal design variables
$\mathbf{x}_{ir}^*$	optimal decision configuration composed of design and operation
$\mathbf{x}_{op}$	operational variables
$\mathbf{x}_{opi}^*$	optimal operation for i^{th} scenario
$\mathbf{y}$	system responses
$\hat{\mathbf{y}}$	system response estimates
y_k	system output at k^{th} time step

$\mathcal{A}$	projected parameter tensor
δ	predicted tip deflection
ρ	atmospheric air density
σ_k	standard deviation of noise at k^{th} time step
χ	offline simulated dataset

Acronyms

AoA	Angle of Attack
DDDAS	Dynamic Data-Driven Application System
DDDEF	Dynamic Data-Driven Estimation Framework
FE	Finite Element
FMM	Fast Multipole Method
GP	Gaussian Process
GPU	Graphics Processing Unit
HOSVD	Higher-Order Singular Value Decomposition
ROPF	Reduced Order Particle Filter
UAS	Unmanned Aerial System
UVLM	Unsteady Vortex Lattice Method
VLM	Vortex Lattice Method

Introduction

Uncertainty in physical responses and changes in environmental conditions will always be limiting factors to reckon with for Unmanned Aircraft System (UAS) performance. Additionally, several recent systems have been and are being designed with long, thin wings to increase efficiency, but with the trade-off of increased susceptibility to aeroelastic effects. In order to increase flight effectiveness, nonlinear aeroelasticity needs to be addressed in the design and operation of such systems. In addition, instabilities and post-instability behavior need to be taken into account. Simulation of these effects does not take into account the uncertainty of operating in a real environment. Hence, once cannot use simulations alone to make truly optimal decisions of mission plans or UAS maneuvers.

The DDDAS has become a popular framework and has been presented in several applications to effectively address these aeroelastic effects in real time. In this framework, one dynamically incorporates data into a running application (e.g., aeroelastic simulator) while simultaneously using the application to steer measurement processes. The main goal of this work was the development of general algorithms for the DDDAS with a specific focus on a joined-wing SensorCraft application (Tilmann, 2002). Nonlinear aeroelastic models are required to capture flutter and other oscillatory behavior that can greatly reduce the operational lifetime of the aircraft. However, these models are computationally expensive. With the DDDAS paradigm, there is an emphasis on increasing simulation speed. Simulations can be performed in advance of a mission in order to predict likely scenarios. Faster calculations means more scenarios can be sampled. Given the variety of scenarios that arise due to unforeseen events in the system and environment, more simulation data can be utilized to predict the expected response of the system. To reduce the computational time during simulations with these models, Graphics Processing Unit (GPU) computing and approximation methods have been and are being investigated. While effective in reducing the computational workload, speedup gained from GPU computing is hardware dependent. This puts a cap on how well it scales with large scale problems.

In the first year, a preliminary DDDAS framework for a decision support system of a joined-wing system was constructed to make use of co-simulation capabilities and optimization under uncertainty. In the second year, the research progress included the modification of the DDDAS framework for a decision support system; construction of flutter stability envelopes for the joined-wing aircraft with and without damage through aeroelastic simulations; development of new data-driven framework for system response prediction; and enhancement of decision support via automated discovery of worst case scenarios for operationally flexible optimization. The focus of this report is mainly on the achievements made in the last year in order to meet the objectives set for this project. In the last year, an algorithmic approach for speeding up the aeroelastic model was developed. A DDDAS framework was built to boost the computational efficiency by incorporating sensor measurements into the simulation. Additionally, data-driven models were investigated to approximate the nonlinear models and thus reduce the number of function calls required. Work was also completed to dynamically improve predictions by assimilating sensor data and data from the nonlinear models. In addition, by using the proposed approach, it was demonstrated through a joined-wing Sensorcraft example that worst-case scenarios for uncertainty could be found in advance to produce an envelope inside which safe UAS operation was possible. Then, in-flight,

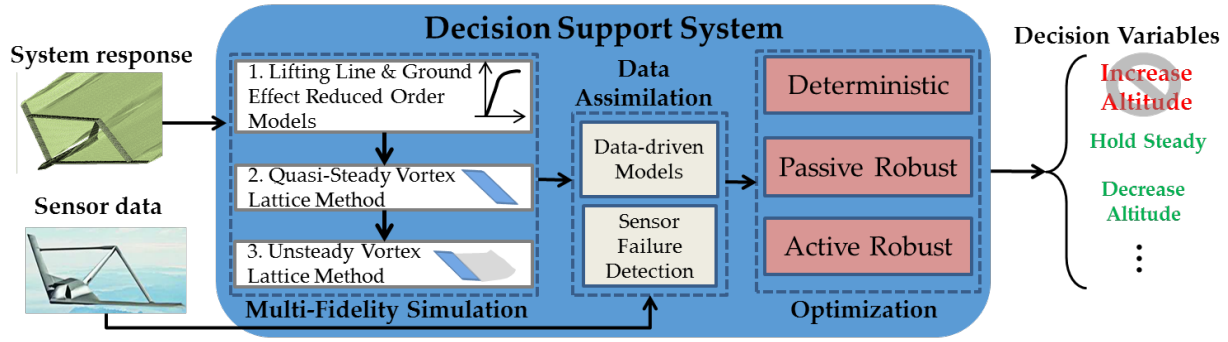

Figure 1: Schematic of decision support system.

sensor data can be used to update the models and allow reoptimization of the maneuvers. In short, faster adjustments with the models to real-time changes of the environment allow suggested maneuvers to be better matched to a current situation.

In this final report, the authors detail the research accomplishments made over the past three and half years toward the overall goal of constructing a decision support system, as outlined in Figure 1. The first year's efforts yielded, an initial DDDAS framework along with a novel UVLM based aeroelastic simulator and an extension of an active robust optimization method to multi-objective problems. The second year effort included studies on the effects of wing damage on flutter speeds, a data-driven model capable of assimilating the online sensor measurement for multi-step-ahead predictions, and a sequential optimization technique for determining necessary scenarios to consider for robustness. The specific goal for the third year's work was to increase the speed of the team's previously developed techniques, and to broaden the scope of the predictions. To accomplish these goals, the aeroelastic simulation was integrated with an algorithm for carrying out efficient computations. The prediction framework was expanded to include spatial effects across the entire UAS. Finally, a surrogate modeling technique for approximating expensive functions was included in the optimization scheme.

The rest of this report is used to highlight the progress made over the past three and a half years. First, the DDDAS framework used is described along with how it can be utilized for prevention of undesired aeroelastic effects. In the next section, the authors detail the aeroelastic model that was developed and analyze the computational costs and how they were reduced. The Dynamic Data-Driven Estimation Framework that was constructed is then provided along with a case study and results demonstrating the efficacy of this framework. Finally, the optimization scheme used to account for the uncertainty and how it can be used for online decision making is explained.

Framework

The framework for the proposed decision support system is shown in Figure 2. This framework consists of both offline and online phases. The offline phase is used for forecasting (e.g., flutter stability and operating range), and in this phase, preliminary mission objectives are used to predict

and optimize the mission performance envelope (e.g., effect of payload on flight duration). In the online phase, dynamic sensor data is to be gathered and processed. This is reflected in Figures 1 and 2. After removal of noise and insignificant data, key data are used in the design of experiments for dynamically improving the prediction models. Some data points are stored and later used for validating the prediction model's accuracy. Based on the prediction models, optimization studies are carried out to determine optimal maneuvers that are feasible with the predicted aeroelastic response. The outcomes are then to be provided to a pilot so that this person may make well-informed decisions on how to proceed further with a maneuver. Previous work by the team focused on the development of the aeroelastic simulation as well as the inclusion of structural damage into the model. In the final stage of the project, the team worked on speeding up the simulations algorithmically. The technique used, the Fast Multipole Method (FMM), is a powerful tool for accelerating calculations between two well separated bodies. In the vortex-based simulation used in this work, the Unsteady Vortex Lattice Method (UVLM), the interactions of pairs of field points and vortex segments are summed up together. This makes it ideal for application of FMM. Integration of UVLM with FMM has been published in the Proceedings of the *2018 SciTech Forum* (Kebbie-Anthony *et al*., 2018) and included in an upcoming publication in the *Journal of Aerospace Information Systems* (Kebbie-Anthony *et al*., 2019).

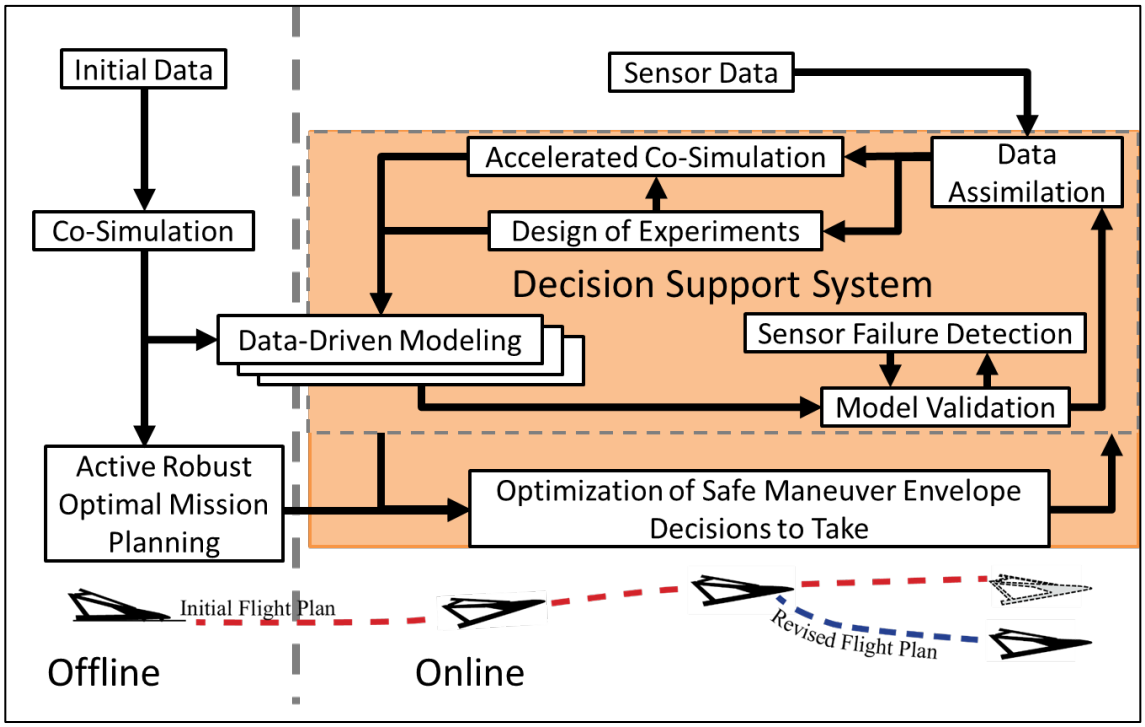

Figure 2: DDDAS framework for decision support system.

Aeroelastic Simulations

The UVLM is used to predict the aerodynamic loads on the lifting surfaces. In order to capture the aeroelastic instabilities, the UVLM is strongly coupled with a structural model to create a co-simulation of aeroelastic dynamics, as also mentioned in last year's report. Co-simulation here

refers to partitioning a coupled system into subsystems that are separately simulated (but numerically integrated) with a suitable exchange of states at predefined time instances to account for the coupling. The two subsystems are computational implementations of models intended for the UAS (joined-wing SensorCraft) structural dynamics and the aerodynamics. The first subsystem, Simulator 1, is associated with the UAS structural model. In Simulator 1, the investigators utilize the Finite Element (FE) method to construct a model with beam elements and simulate the motions of the wings of a representative UAS (joined-wing SensorCraft). The motion of the joined-wing SensorCraft through space and time is determined by using the mass and stiffness matrices along with the load vector (which will be obtained from Simulator 2). In Figure 3, the beam element representation of the left forward and rear wings of a representative joined-wing SensorCraft is shown. The beam nodal points, which are represented by circles in Figure 3, are distributed along the elastic axes of the wings. The distributed mass of the wings is discretized and concentrated at the nodal points. The second subsystem, Simulator 2, is the aerodynamic model. In Simulator 2, the investigators utilize the UVLM to simulate the aerodynamic loads acting on the representative joined-wing SensorCraft. The wake, a vorticity containing region, is convected behind the aircraft. Through the convection of the wake, the aerodynamic loads (lift and drag) for the system are estimated. The mesh used for the aerodynamic model of the full joined-wing aircraft is shown in Figure 4. To capture the aerodynamic effects with the highest fidelity level, a refined mesh is used. More information on the co-simulation can be found in the work of Roccia, Preidikman, and Balachandran (2017) and Preidikman *et al*. (2017).

The major source of computational complexity in the aerodynamic model used for this work was determined to lie in the computation of the wake velocities. This behavior can be observed in the aeroelastic simulation of a representative joined-wing SensorCraft, as shown in Figure 5. In Figure 5, it is shown that over 90% of the computation time involved in the aeroelastic simulation for large domain sizes of the joined-wing SensorCraft is spent in evaluating the wake velocity field. The computational time required to compute the structural response; that is, to numerically integrate the structure's equations of motion, is negligible in the comparison chart since it is dwarfed by the aerodynamic calculations. For similar reasons, certain processes of the

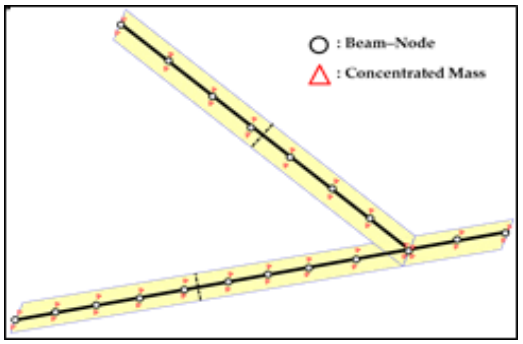

Figure 3: Beam element representation of joined-wing aircraft wing. The left forward wing and the the left rear wing are shown in the figure.

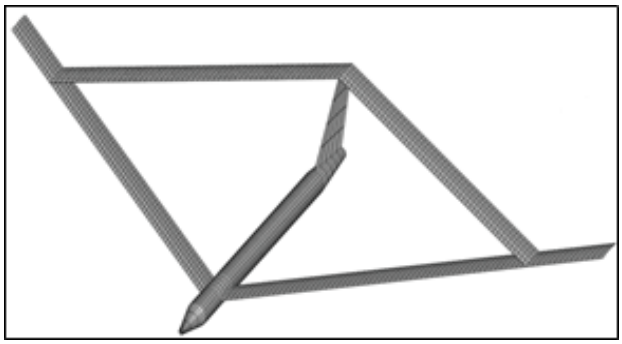

Figure 4: Aerodynamic grid for full joined-wing aircraft. This grid is made for the right and left rear wings, right and left forward wings, vertical tail, and fuselage.

aerodynamic model involving the evaluation of the vortex circulations and the loads are not shown. This dominating effect of the velocity calculations emphasizes the need for acceleration of the wake velocity computations in the aerodynamic model to accelerate the entire aeroelastic simulation.

The algorithm adopted here to attain this acceleration is the FMM. The FMM is a hierarchical algorithm, which can be used to speed up matrix-vector products. The main concept behind the FMM is that the interactions within the system can be classified into two groups, the near-field (sparse matrix-vector product) and far-field (dense matrix-vector product) interactions. The near-field interactions are computed directly, while the far-field interactions are approximated via the use of data structures, the generation of multipole expansions, and the evaluation of local expansions. It can be mentioned that a number of parameters, such as the truncation number, the order of quadrature, and the clustering parameter (or the maximum octree level) can be used to tune the speed of the FMM. There are opportunities to "trade" accuracy for speed by varying these parameters, which also can be optimized for the required accuracy. The FMM accuracy should be set based on the desired overall accuracy of the simulation, and, in principle, should be determined by using data on the time marching schemes, the mesh size, and other parts of the UVLM to have a stable and consistent overall approximation.

To quantify the speed increase, the complexity of the UVLM algorithm can be estimated, by individual components and its overall computational complexity with and without the FMM. Consider the case of a relatively small body mesh of size N_b, which is fixed and the mesh representing the vortex sheets of size N, which is growing in time. Since at each time step, vorticity is shed from the trailing and outer edges of the body, the complexity for the k^{th} time step

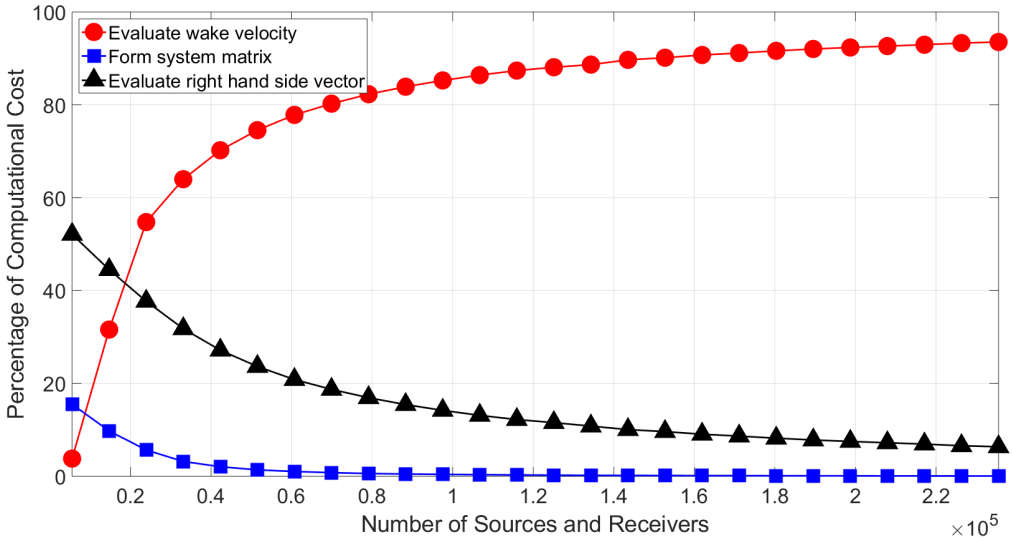

Figure 5: Percentage of the total computational cost of aeroelastic simulator from aerodynamic model processes: evaluation of wake velocity (circles), formation of system matrix (squares), and evaluation of the right hand side vector (triangles).

Table 1: Estimation of computational complexity of the UVLM processes with and without FMM

Step	Without FMM (per time step)	With FMM (per time step)	Without FMM (K time steps)	With FMM (K time steps)
Form system matrix	$O\left(N_b^2\right)$	$O\left(N_b^2\right)$	$O\left(N_b^2\right)$	$O\left(N_b^2\right)$
Evaluate right hand side vector	$O\left(N_b N\right)$	$O\left(N_b + N\right)$	$O\left(N_b^{3/2} K^2\right)$	$O\left(N_b K + N_b^{1/2} K^2\right)$
Solve linear system	$O\left(N_b^3\right)$	$O\left(N_b^3\right)$	$O\left(N_b^3 K\right)$	$O\left(N_b^3 K\right)$
Evaluate wake velocity	$O\left(N_b N + N^2\right)$	$O\left(N_b + N\right)$	$O\left(N_b^{3/2} K^2 + N_b K^3\right)$	$O\left(N_b K + N_b^{1/2} K^2\right)$
Evolve mesh	$O\left(N_b + N\right)$	$O\left(N_b + N\right)$	$O\left(N_b K + N_b^{1/2} K^2\right)$	$O\left(N_b K + N_b^{1/2} K^2\right)$
Total	$O\left(N_b^3 + N^2\right)$	$O\left(N_b^3 + N\right)$	$O\left(N_b^3 K + N_b K^3\right)$	$O\left(N_b^3 K + N_b^{1/2} K^3\right)$

can be estimated as $N = O\left(N_b^{1/2} k\right)$, so, the total complexity to compute K steps is a sum of the complexities for $k = 1, \cdots, K$. In Table 1, the authors show the computational complexity estimates for each component of the UVLM algorithm. It can be seen that the use of the FMM reduces the complexity of the calculations of the right hand side vector and wake velocity. Complexity at large values of K grows at $O\left(K^2\right)$ as opposed to $O\left(K^3\right)$ for the standard UVLM.

In Figure 6, the results are depicted for the speed tests of the UVLM with and without the FMM for the individual time steps. In Figure 6, the computational time for the evaluation of the wake velocity fields of the UVLM is plotted against the number of time steps. On a logarithmic scale, the slope of the dashed line is 2, which indicates the computational complexity of the standard UVLM evaluation of wake velocities for large values of K is of $O\left(K^2\right)$ where K is the total number of time steps. The slope of the computational complexity of the FMM accelerated UVLM is indicated by the dotted line, which has a slope of 1 (*i.e.*, grows proportionally with K). Thus, with the inclusion of the FMM, the computational complexity of the evaluation of wake velocities was reduced from $O\left(K^2\right)$ to $O\left(K\right)$. Note that the FMM accelerated UVLM only begins to outperform the standard UVLM after about $k = 8$ time steps (approximately $N = 1,500$ sources). This improvement in speed is achieved with no noticeable loss in accuracy. The relative L_2-norm error of the computed wake velocities of the FMM accelerated UVLM is of the order $\sim 10^{-5}$.

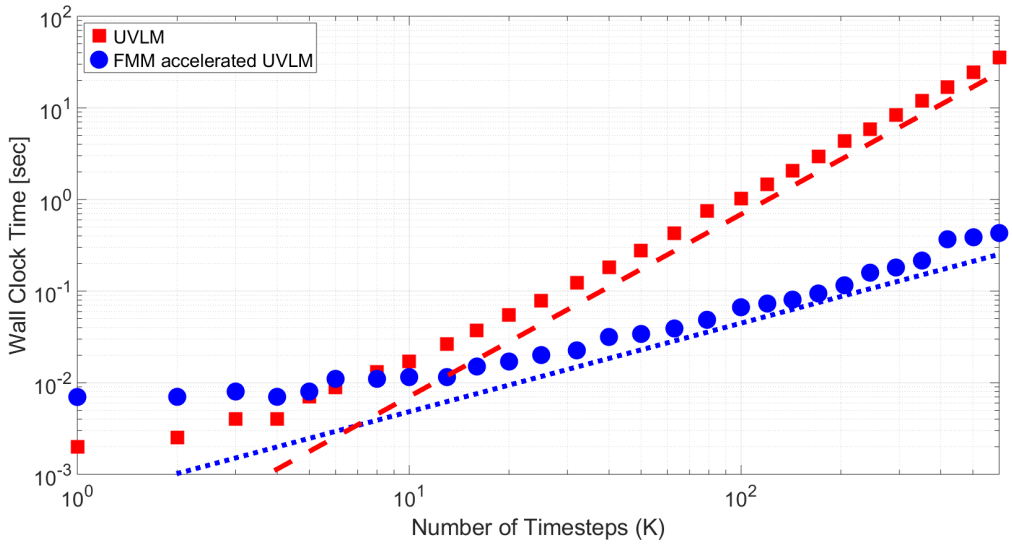

Figure 6: Wall clock time for the evaluation of wake velocity in UVLM with and without the FMM for the individual time steps. With the dashed line, the authors show the quadratic dependence of the UVLM, and with the dotted line, they show the linear dependence of the FMM accelerated UVLM.

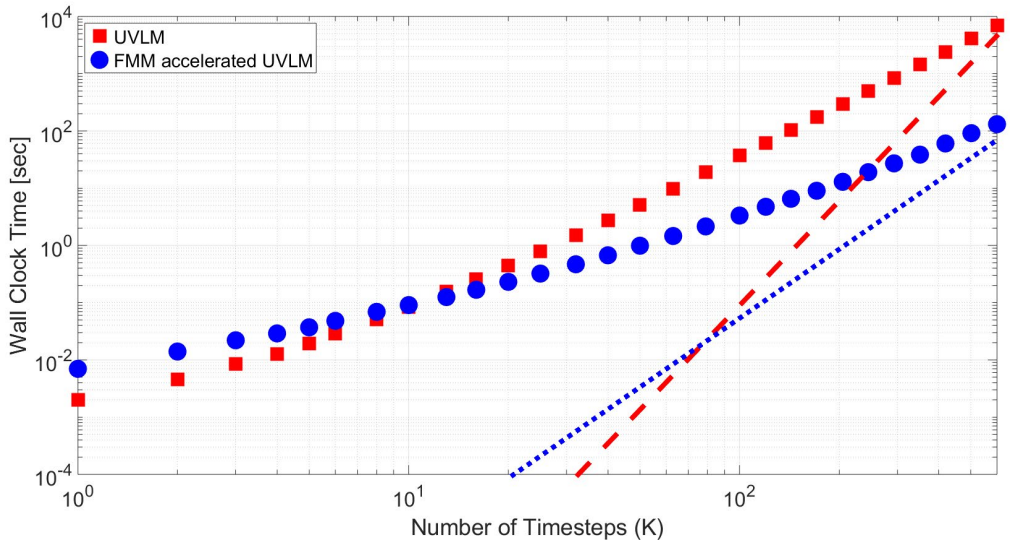

Figure 7: Wall clock time for the evaluation of wake velocity in UVLM with and without the FMM for the cumulative time steps. With the dashed line, the authors show the cubic dependence of the UVLM, and with the dotted line, they show the quadratic dependence of the FMM accelerated UVLM.

In Figure 7, the results are depicted of the speed tests of the UVLM with and without the FMM for the cumulative time steps. For significantly large K, the computational complexity of the

standard UVLM evaluation of wake velocities is of $O\left(K^3\right)$, while the computational complexity of the FMM accelerated UVLM evaluation of wake velocities is of $O\left(K^2\right)$. The computational savings from the FMM will allow for larger numbers of operating conditions to be simulated. For the prediction framework in the following section, this corresponds to a greater number of available data sets on which to train. More available data sets can be leveraged for greater prediction accuracy, benefitting the whole decision support system. The FMM has been used to reduce the computational expense of the velocity field computations from $O\left(K^3\right)$ to $O\left(K^2\right)$. The significant acceleration allows for simulation domain sizes that were previously computationally intractable. Thus, modeling a more complex systems, such as the joined-wing SensorCraft, to attain aeroelastic responses becomes more practical.

Dynamic Data-Driven Estimation Framework (DDDEF)

In prior years' work, the authors produced a data-driven framework to integrate multiple local sensor measurements with the quasi-steady Vortex Lattice Method (VLM) for a system-wide (global) state estimate. The addition of sensor measurements has been used to attain consistent improvement for the prediction accuracy over the VLM for quasi-steady system responses (Kania *et al*., 2017). To capture flutter effects, especially post-flutter behavior, an unsteady model, such as the UVLM based aerodynamic model, is required. This work has been extended by dynamically incorporating sensor measurements into the UVLM for predicting local aeroelastic responses (Zhao *et al*., 2018a, Zhao *et al*., 2019). Then, through further effort, this estimation framework was extended for predicting global system behavior (spatiotemporal) with sparse sensor measurements and applied to a flutter prediction case study (Zhao *et al*., 2018b).

To construct a decision support system, it is crucial to have a fast and a reasonably accurate system prediction environment based on the current flight conditions. The focus of this work has been on the prediction of aeroelastic responses for a joined-wing aircraft, which vary spatially along its wing structure as well as change over time. As mentioned in the previous section, the UVLM based aerodynamic model can be used to obtain an accurate prediction of the system's aerodynamic behavior. However, due to the computational expense, it is impractical to use the aeroelastic simulator for online predictions. Additionally, with sensors, one can collect a continuous stream of environmental and structural response data from the aircraft. Since the sensors considered here can only provide measurements of the region local to them, they are insufficient for capturing the behavior of the whole system. One objective of this research is to develop dynamic spatiotemporal prediction models through combination of the aeroelastic simulator and sensor measurements, to achieve high computational efficiency as well as comparable accuracy to the high-fidelity simulation.

The proposed framework in Zhao *et al*. (2018b), a schematic of which is shown in Figure 8, is composed of an offline phase and an online phase. In the offline phase, the essential idea is to construct a meta-model to directly predict system aeroelastic responses from available offline simulation data sets. The prediction is achieved through a combination of higher-order singular value decomposition and a Gaussian process. First, Higher-Order Singular Value Decomposition

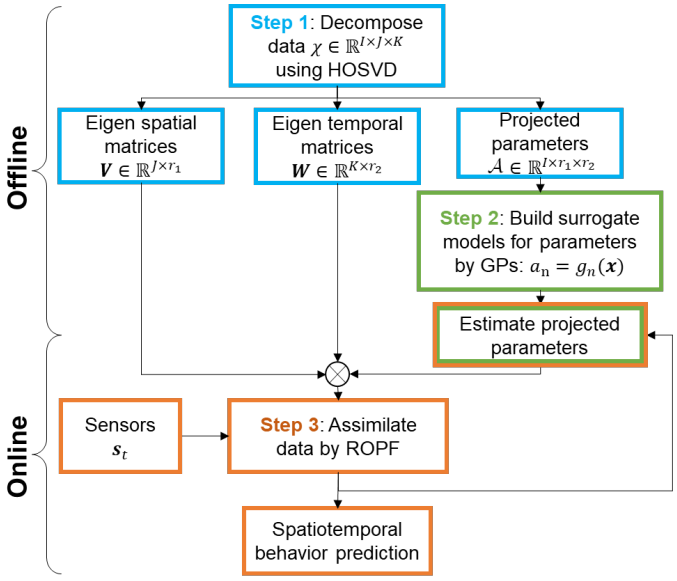

Figure 8: Framework for proposed approach.

(HOSVD) is applied to decompose the multi-dimensional simulation results into eigen spatial and temporal matrices, and a set of low-dimensional projected parameters. Then, Gaussian Process (GP) models, trained on the projected parameters obtained from the first step, are employed to interpolate aeroelastic responses for known flight conditions. Together those eigen matrices and the GP models are stored offline for making a prior spatiotemporal prediction during online operation. For the third step, the reduced-order particle filter is utilized to assimilate sparse sensor measurements to iteratively enhance the prediction of the projected parameters. Thus, by integrating updated parameters with eigen spatial and temporal matrices, efficient enhancement for spatiotemporal predictions can be attained. The proposed framework is exemplified by the following case study.

While the proposed approach in this section is general, the system studied for an application of the approach was the previously mentioned, joined-wing SensorCraft. The offline model is the aeroelastic simulator from the previous section. The inputs considered for the aeroelastic simulator are three different physical parameters of flight. They are the freestream velocity's magnitude (airspeed), angle of attack, and atmospheric air density. The outputs of interests are the time-varying nodal displacements at 19 discrete locations on the left wing of the aircraft, where the locations are indicated as $\{\mathbf{d}_i\}_{i=1}^{19}$ in Figure 9. During the offline stage, the available datasets consist of 9 aeroelastic simulation results at different operating conditions, given in Table 2, all within the post-flutter regime (after the onset of flutter). Here, the sensors' data are assumed to be available for sparse measurements of the nodal displacements along the vertical direction. The spatial locations of each sensor are arbitrarily selected from the 19 simulated locations, as indicated by the green circles in Figure 9.

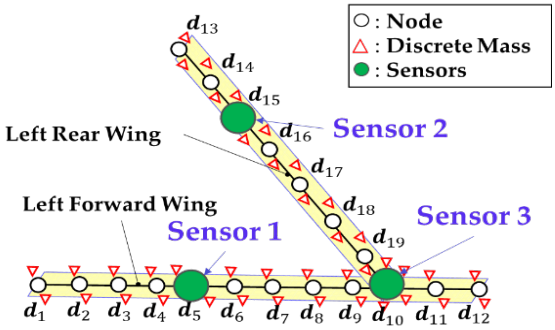

Figure 9: Aeroelastic simulation model: beam representation of left wing of the joined-wing SensorCraft.

Table 2: Nine operating conditions used in aeroelastic simulations

Simulation Data Set	Freestream Velocity $V\,[m/s]$	Angle of Attack $AoA\,[^o]$	Air Density $\rho\,[kg/m^3]$
1	160	5	1.152
2	161	5	1.152
3	162	5	1.152
4	163	5	1.152
5	164	5	1.152
6	165	5	1.152
7	170	10	1.152
8	175	10	1.152
9	180	5	1.152

The preliminary prediction of the time-varying nodal displacement obtained from the first two steps are depicted in Figure 10. In Figure 10(a), the authors show the contour plot of simulated nodal displacements at 19 locations for 1,000 time steps by the prescribed aeroelastic simulator. Then, the prior predictions computed from the deposited offline models are illustrated in Figure 10(b). Meanwhile, the absolute prediction errors between the aeroelastic simulator results and the initial estimate are demonstrated in Figure 10(c). It can be seen that initial predictions can provide reasonably accurate estimations of nodal displacements for majority of the spatial locations, including locations $\mathbf{d}_1$ to $\mathbf{d}_{13}$. Only small magnitude and phase differences are notable among these locations. However, the estimates among locations between $\mathbf{d}_{14}$ and $\mathbf{d}_{19}$; that is, the aircraft's left rear wing, have noticeable prediction errors mainly due to magnitude and phase differences.

The online prediction procedure is achieved via the Reduced Order Particle Filter (ROPF), in which a standard particle filter is integrated with HOSVD to reduce the computational complexity for assimilating the sensor measurements with the simulation data (Zhao *et al.*, 2018b). Three representative results obtained during the procedure are shown in Figure 11. In this figure, the authors show the contour plots of absolute prediction errors at the 5th, 100th, and 200th assimilation

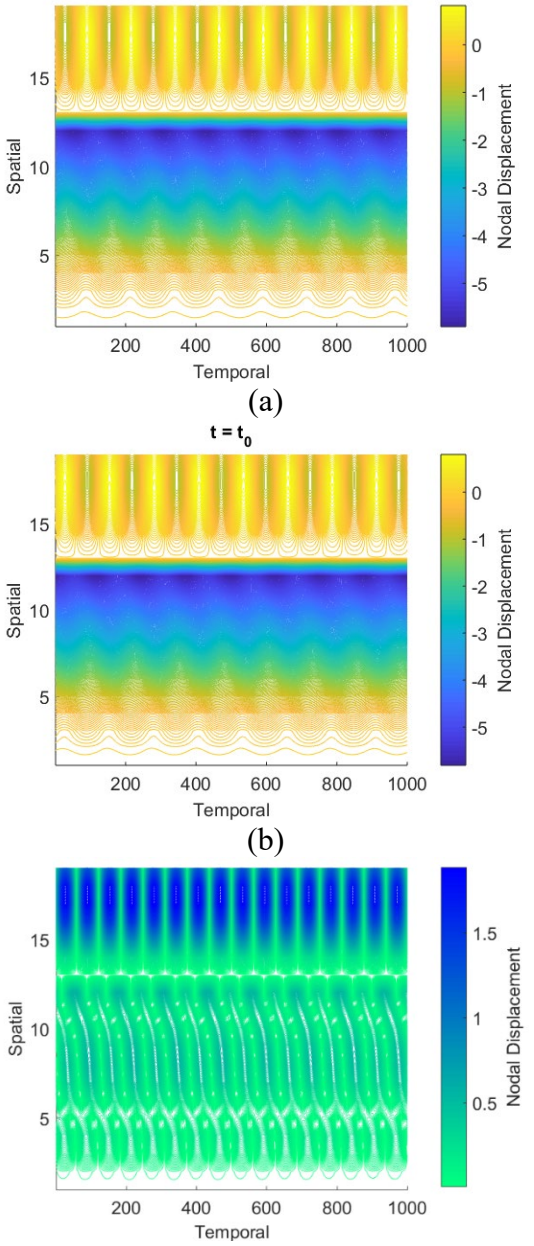

Figure 10: Initial prediction at $k = k_0$ (a) simulated system behavior, (b) offline model prediction, and (c) predicted absolute error.

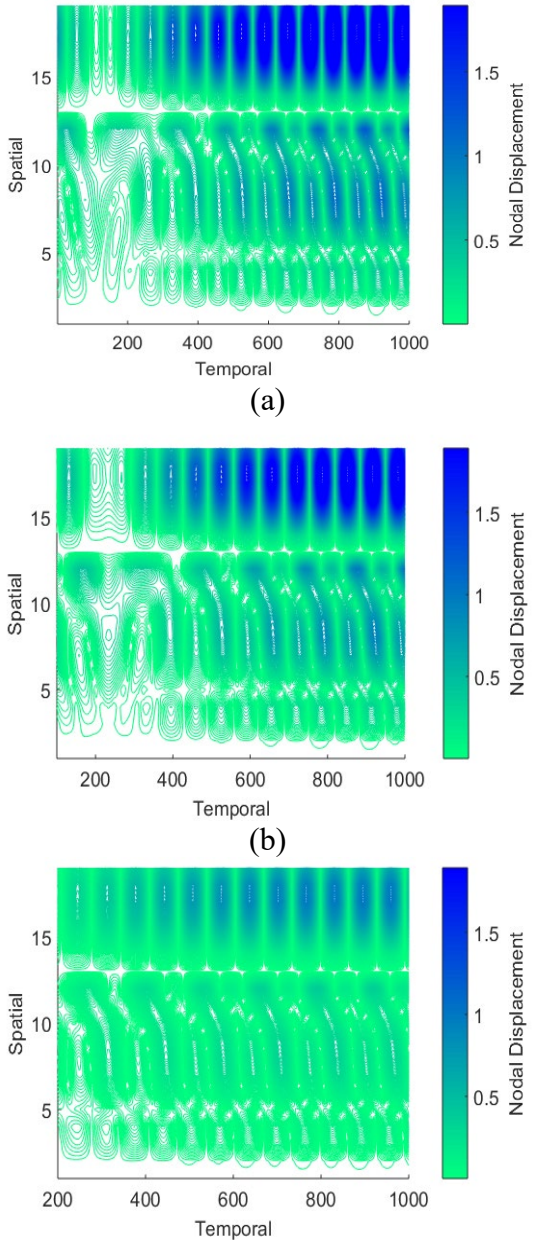

Figure 11: Online data assimilation process: the absolute prediction errors at (a) $k = k_5$ (b) $k = k_{100}$, and (c) $k = k_{200}$.

Table 3: Average absolute and relative prediction error for 9 flight conditions

Conditions	1	2	3	4	5
Absolute error	0.059	0.056	0.064	0.058	0.059
Relative error	4.37%	4.12%	4.64%	4.13%	4.14%

Conditions	6	7	8	9	Mean
Absolute error	0.051	0.049	0.052	0.054	0.056
Relative error	3.53%	2.11%	2.15%	3.21%	3.60%

cycles separately. After five assimilation iterations, as displayed in Figure 11(a), the prediction error for the first 200 time steps has largely reduced amongst all the spatial locations, in contrast to the prior prediction error in Figure 10(c). However, these predictions still decay as they extend further into the future. As the 100^{th} time step is reached by the assimilation process, an additional deduction of prediction errors for the first 400 time steps can be perceived in Figure 11(b). However, there still exists discernible errors between locations $\mathbf{d}_{14}$ and $\mathbf{d}_{19}$. The results obtained after reaching the 200^{th} assimilation iteration are shown in Figure 11(c). The prediction errors for all the spatial locations as well as the subsequent 800 time steps have significantly decreased.

The final prediction results obtained for each of the nine flight conditions are provided in Table 3. The average absolute prediction errors are shown along with the relative errors with respect to the nonlinear aeroelastic simulator results. Through the proposed framework, the authors demonstrate the predictive capability comparable to that of the high-fidelity simulation, with all of the relative errors being within 5%. With the results obtained for the joined-wing SensorCraft case study, it can be stated that one can use the predictive framework to predict the global aeroelastic responses with comparable accuracy to high-fidelity simulations, while significantly reducing the computational cost. In addition, the effect of sensor placement configuration on the prediction performance has been further investigated, and from this study, it is gathered that the predictions are relatively robust to sensor locations. Hence, it is envisioned that the proposed methodology can be efficiently used for online optimization.

Optimization

From the previous section, one can gather that efficient predictions of the aeroelastic response can serve in the decision making of the system for selection of maneuvers in response to environmental changes. Since there is always inherent uncertainty in predictions of environmental changes, a goal of the work pertaining to this section is to provide optimal maneuvers that are robust (relatively insensitive) to uncertainty. Flexible optimization is one promising approach for this problem, through which one can find an optimal design, considering that the outcome of uncertain events are known and the effects on the system are mitigated through subsequent operations. However, it is computationally intractable for almost any nontrivial nonlinear optimization problem. In previous years' efforts, the authors found that discretizing the problem could greatly reduce the costs (Azarm and Lee, 2016). The discretized approach is the most beneficial when something is known about the relationship of the function being optimized and the uncertain parameters. If not, an arbitrarily fine discretization can quickly result in an intractable problem. To address this,

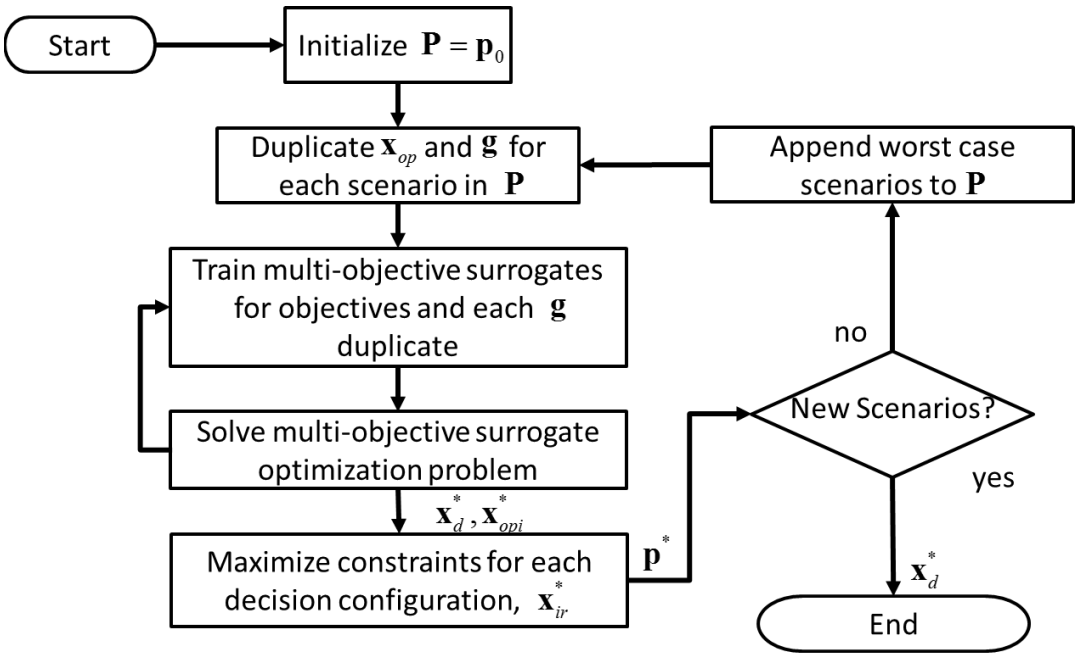

Figure 12: Framework for sequential active robust optimization with surrogate modeling.

subsequent research efforts, the authors sought to iteratively solve the flexible optimization problem. By searching for the worst cases that lead to constraint violations, only necessary scenarios are considered, and the parameters need not be overly discretized, keeping the problem to a manageable size. To further the computational efficacy, the final year's efforts were focused on integration with surrogate optimization.

The iterative surrogate algorithm for multi-objective optimization is shown in Figure 12. To begin, the set of uncertain scenarios is initialized with the most likely (nominal) values of each uncertain parameter. Each iteration of the sequential discretized flexible optimization will result in addition of new worst-case scenarios. For each set of parameters, representing a distinct worst-case scenario, a corresponding operation vector and instance of the constraints is generated. Each operation variable represents a reactive operation that can be performed to mitigate the effects of one of the worst-case scenarios. Surrogate models are then trained for all of the objective and constraint functions. The initial training is performed over points selected by a random design of experiments. Kriging models are fitted to the data via maximum likelihood criteria (Forrester *et al*., 2007). Once the models have been trained, they can be exploited to approximate values of candidate configurations without evaluating the expensive function. Such configurations are identified by using the surrogate to estimate which one will have the greatest expected improvement over current solutions. The new candidate point is then evaluated and the models are trained over them. The added points simultaneously refine the models and help move towards the optimal values. The final result of the surrogate exploitation is a set of optimal designs, decisions made before realization of the uncertain parameters, and operations, decisions made after the

uncertain parameter to mitigate its effects, which satisfy all constraints for all known scenarios. The optimal values are then tested for their robustness. For every non-dominated solution, dominated solutions being those that are less optimal than at least one other point with respect to all objectives considered, on the Pareto frontier the constraints are maximized with respect to the uncertain parameters for each optimal configuration. In this way, all worst-case scenarios can be identified. Each new worst case is added to the set of worst-case scenarios and the next iteration is begun. The process terminates when no new worst-case scenarios are found, and all known scenarios can produce feasible optima.

Applications for active robust optimization are largely restricted to design optimization (Cardin, 2014). In such a case, the design is optimized to be robust to uncertain events by considering operations or actions that can be taken after the event. Active robust optimization can also be used for online decision making by instead viewing the design as the current action and the operations as future actions. In this way, an active robust receding horizon scheme can be formulated. In the scenario tree of Figure 13, the authors show the decisions $\mathbf{x}_k$ in relation to the uncertain event realizations $\mathbf{p}_{k,i}$. Note that the scenarios at time k affect the scenarios at all future time steps. This is reflected in the scenario tree by denoting the scenarios with indices for the time step in which they occur and the sequence of scenarios preceding it.

As a case study, the optimization of a safe maneuver envelope for a SensorCraft is considered to demonstrate the proposed approach as decision support. The goal is to determine what maneuver to perform at the current time to ensure optimal maneuvers at future times regardless of uncertainty. The specific objectives are maximization of the airspeed and angle of attack. The time dependent data-driven model discussed in the previous section is used to predict the system response as a function of the airspeed V and angle of attack AoA. The problem is constrained by a limit to the amount of tip deflection δ predicted by the model $\hat{\delta}$ to within a maximum deflection of $\delta_{\max}$ .Three discrete decision times $k = 1,2,3$ are considered for the optimization with two random events occurring between them, represented by the scenario tree in Figure 13. Here, the uncertain event is a measurement of the actual wind speed, which can vary by the amount ΔV that has the lower bound ΔV_l and the upper bound ΔV_u. The first of the three decisions corresponds to the current action to undertake, and the second and third correspond to future actions to be made after the uncertain events. A second constraint is used to impose the physical reality that velocity can be changed a limited amount $V_{\lim}$between time steps. The results are provided in Figure 14.

$$\max_{V_{0,i},\, V_{k,i}} E_i\left[\frac{1}{k}\sum_{k=0}^{K} V_{k,i}\right],\ \max_{AoA_{0,i},\, AoA_{k,i}} E_i\left[\frac{1}{k}\sum_{k=0}^{K} AoA_{k,i}\right]$$

$$s.t.\ \ \hat{\delta}(V_{k,i} + \Delta V_{k,i}, AoA_{k,i}) \leqslant \delta_{\max}$$

$$\left|V_{k,i} - V_{k+1,i}\right| \leqslant V_{\lim}$$

$$\forall k = 0,\ldots,K$$

$$\forall \Delta \mathrm{V}_{k,i} \in [\Delta V_l, \Delta V_u]$$

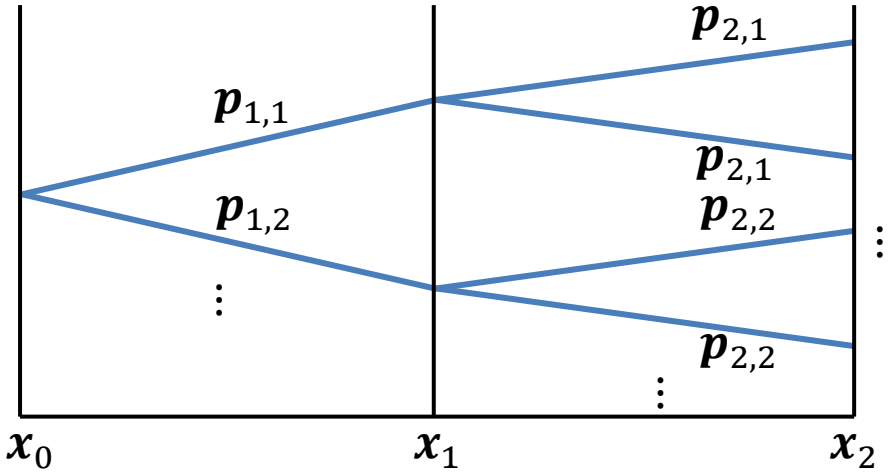

Figure 13: Scenario tree showing three decisions and two uncertain events.

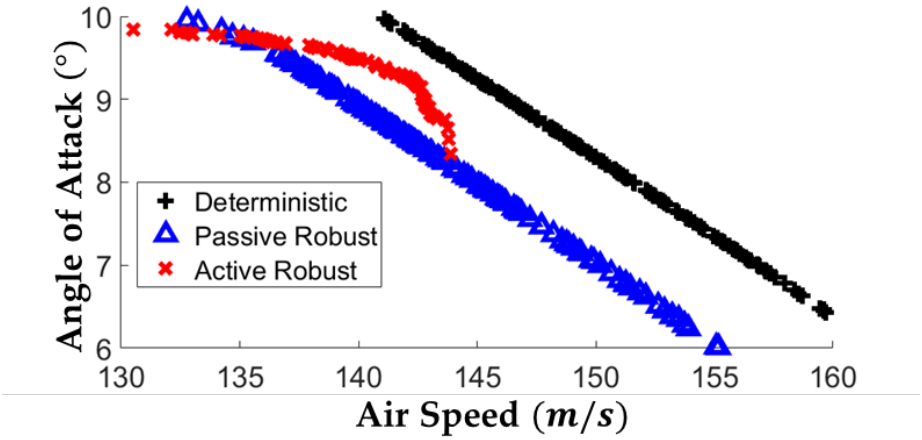

Figure 14: Pareto frontiers for the case study using the Deterministic, Passive Robust, and Active Robust optimization techniques.

The case study was performed at five scenarios for the passive and active robust methods and nominal parameter values for the deterministic case. The problem was solved by using a multi-objective genetic algorithm. Each point on the Pareto frontiers in Figure 14 represents an optimal maneuver, for the two maximizing objectives. With deterministic optimization, one predicts the best response for its solutions, but this technique does not guarantee robustness for any values of uncertainty other than the nominal. The passive robust solutions are more conservative but are guaranteed to be feasible regardless of the uncertain events. Similarly, the active robust solutions are maneuvers that can be made feasible with future maneuvers for any outcome. Since, it allows for future corrections, the active robust method produces less conservative results. By using this method for decision support, better solutions can be found and utilized.

Concluding Remarks

In the work presented here, the team has summarized the research outcomes obtained over the last 3.5 years on the development of a decision support system in the DDDAS paradigm. The DDDAS framework for the decision support system has been enhanced for faster computational speed, and efficient global aeroelastic response prediction. Through integration of the FMM with the most expensive UVLM aerodynamic computations, namely, the evaluation of wake velocity, the authors have shown that greater control can be obtained over the trade-off between accuracy and speed. The DDDEF was developed and has been shown capable of predicting the global aeroelastic response for low computational cost. With computationally cheaper function evaluations, online optimization can be feasible. Additionally, incorporating measures of robustness that take operational variables into account would mean that the resulting decision support system could help pilots realize efficient performance with thin, flexible wing aircraft such as the joined-wing SensorCraft.

Interactions and Collaborations

During the course of this project, the investigators shared their findings with Dr. Phil Beran and Dr. Ravi Chona of the Air Force Research Laboratory (AFRL), and Dr. Hamilton S. Brown (Sensors Directorate, AFRL), Wright Patterson Base, Dayton, OH, Dr. Yu-Tai Lee of the Naval Surface Warfare Center, Carderock, MD, Drs. Walt Silva and Robert Scott of the NASA Langley Research Center, Hampton, VA, Dr. Robert Canfield of Virgnia Tech, Blacksburg, VA, Professor Richard Fujimoto of Georgia Tech, and Professor Aniruddha Gokhule of Vanderbilt University. In addition, for some of the SensorCraft related data, the team members had extended interactions with researchers in the AFRL supported Collaborative Center for Multidisciplinary Sciences at Virginia Tech, Blacksburg, VA. In addition, the team had a collaboration with Professor Sergio Preidikman of the National University of Cordoba, Argentina on UVLM studies and fluid-structure simulations. The team has also collaborated with Dr. Nail Gumerov and Professor Ramani Duraiswami from the University of Maryland Institute of Advanced Computer Studies on the use of the fast multipole method to accelerate the UVLM studies.

References

1. Hu, W., Li, M., Azarm, S., and Almansoori, A. (2011). "Multi-Objective Robust Optimization under Interval Uncertainty Using Online Approximation and Constraint Cuts." *Journal of Mechanical Design*, *133*(6), 061002.
2. Tilmann, C. P. (2002). "Emerging Aerodynamic Technologies for High-Altitude Long-Endurance SensorCraft UAVs." *Air Force Research Lab Wright-Patterson AFB OH Air Vehicles Directorate*. Retrieved from http://www.dtic.mil/get-tr-doc/pdf?AD=ADA428754
3. Forrester, A., Sobester, A., & Keane, A. (2008). *Engineering design via surrogate modelling: a practical guide*. John Wiley & Sons.
4. Cardin, M. A. (2014). Enabling flexibility in engineering systems: a taxonomy of procedures and a design framework. *Journal of Mechanical Design*, *136*(1), 011005.

Publications

1. Roccia, B., Preidikman, S., and Balachandran, B. (2017) "Computational Dynamics of Flapping Wings in Hover Flight: A Co-Simulation Strategy." *AIAA Journal*, Vol. 55, No. 6, pp. 1806-1822. http://dx.doi.org/10.2514/1.J055137.
2. Preidikman, S., Roccia, B., Verstraete, M., Valdez, M., Mook, D., and Balachandran, B. (2017). Computational Aeroelasticity of Flying Robots with Flexible Wings. In *Aerial Robots – Aerodynamics, Control and Applications,* Chapter 1. INTECH. http://dx.doi.org/10.5772/intechopen.69396 .
3. Zhao, X., Kebbie-Anthony, A., Azarm, S., and Balachandran, B., (2019). "Dynamic Multi-step-ahead Prediction with Sensor Observation," *AIAA Journal* [To appear].
4. Kebbie-Anthony, A., Gumerov, N., Preidikman, S., Balachandran, B., and Azarm, S. (2019). "Fast Multipole Accelerated Unsteady Vortex Lattice Method," *Journal of Aerospace Information Systems* [To Appear].
5. Kania, R., Kebbie-Anthony, A., Zhao, X., Azarm, S., and Balachandran, B. (2018). Dynamic Data-Driven Approach for Unmanned Aircraft Systems and Aeroelastic Response Analysis. In *Handbook of Dynamic Data Driven Applications Systems* (pp. 193-211). Springer, Cham.
6. Zhao, X., Azarm, S., and Balachandran, B., (2018b). "Dynamic Data-Driven Spatiotemporal System Behavior Prediction with Simulations and Sensor Measurement Data," In *ASME 2018 International Design Engineering Technical Conferences and Computers and Information in Engineering Conference*, pp. V02BT03A060-V02BT03A060. American Society of Mechanical Engineers.
7. Kebbie-Anthony, A., Gumerov, N., Preidikman, S., Balachandran, B., and Azarm, S. (2018). "Fast Multipole Method for Nonlinear, Unsteady Aerodynamic Simulations," In *2018 AIAA Modeling and Simulation Technologies Conference*, AIAA 2018-1929.
8. Zhao, X., Kania, R., Kebbie-Anthony, A., Azarm, S., and Balachandran, B., (2018a). "Dynamic Data-Driven Aeroelastic Response Prediction with Discrete Sensor

Observations," In *2018 AIAA Modeling and Simulation Technologies Conference*, AIAA 2018-2173.

9. Azarm, S. and Lee, Y.-T. (2016) "Multi-Objective Robust Optimization Formulations with Operational Flexibility and Discretized Uncertainty." In *Proceedings of the International Design Engineering Technical Conferences*, pp. V02BT03A052-V02BT03A052. Charlotte, NC, August 21-24.
10. Kania, R., Azarm, S., and Balachandran, B. (2016) "Use of Operationally Flexible Robust Optimization in Dynamic Data Driven Application Systems." *InfoSymbiotics/Dynamic Data Driven Application Systems Conference*, Hartford, CT, August 9.